Controlling the Spin of Co Atoms on Pt(111) by Hydrogen Adsorption

Q. Dubout,[1] F. Donati,[1] C. Wäckerlin,[1] F. Calleja,[1,2] M. Etzkorn,[1,3] A. Lehnert,[1] L. Claude,[1]
P. Gambardella,[1,4] and H. Brune[1]

[1]*Institute of Condensed Matter Physics (ICMP), École Polytechnique Fédérale de Lausanne (EPFL),
Station 3, CH-1015 Lausanne, Switzerland*
[2]*Madrid Institute for Advanced Studies, IMDEA Nanoscience, Calle Faraday 9, Campus Cantoblanco,
E-28049 Madrid, Spain*
[3]*Max Planck Institute for Solid State Research, Heisenbergstrasse 1, 70569 Stuttgart, Germany*
[4]*Department of Materials, ETH Zürich, Hönggerbergring 64, CH-8093 Zürich, Switzerland*
(Received 22 December 2014; published 11 March 2015)

We investigate the effect of H adsorption on the magnetic properties of individual Co atoms on Pt(111) with scanning tunneling microscopy. For pristine Co atoms, we detect no inelastic features in the tunnel spectra. Conversely, CoH and CoH_2 show a number of low-energy vibrational features in their differential conductance identified by isotope substitution. Only the fcc-adsorbed species present conductance steps of magnetic origin, with a field splitting identifying their effective spin as $S_{eff} = 2$ for CoH and $3/2$ for CoH_2. The exposure to H_2 and desorption through tunnel electrons allow the reversible control of the spin in half-integer steps. Because of the presence of the surface, the hydrogen-induced spin increase is opposite to the spin sequence of CoH_n molecules in the gas phase.

Individual surface-adsorbed magnetic atoms exhibit remarkably large orbital moments and anisotropies [1–5]. Like in adsorbed single ion molecules [6–10], their chemical environment can be tailored through exposure to reactive molecules, thus allowing the tuning of their magnetic properties [11]. Among the wealth of available molecules, H_2 is of particular interest. The high reactivity of adsorbed transition metal atoms promotes the dissociation of the H_2 molecule and the formation of metal-H_n complexes ($n = 1, 2, 3$), even at cryogenic temperatures [2,12–16]. Moreover, the relatively small H desorption barrier allows the reversible control of the number of adsorbed hydrogen atoms, e.g., by desorption through electrons from a scanning tunneling microscopy (STM) tip and adsorption from the gas phase [2,15].

The magnetic properties of gas phase transition-metal-H_n complexes have been studied by means of *ab initio* calculations. These calculations reveal a significant change of the magnetic properties through hydrogenation, with a clear tendency of decreasing spin with increasing number of H atoms [17–19]. This results from the antiparallel spin alignment between metal and H. In particular, for the case of Co, the spin $S = 3/2$ of the free atom is reduced to 1 and $1/2$ upon the adsorption of one and two hydrogen atoms, respectively [17–19].

The effect of hydrogen adsorption on the spin of surface-adsorbed magnetic atoms is largely unknown. Hints that the spin possibly changes upon H adsorption can be inferred from the H-induced appearance [14] or disappearance [13,15] of the Kondo effect. However, for $S > 1/2$ this can also be caused by a change in magnetic anisotropy [20].

Neither the spin nor the anisotropy have been measured in Refs. [13–15], while for Co/graphene/Pt(111) the adsorption of three H atoms was shown to reduce the anisotropy energy [2].

Here we demonstrate that the spin of individual Co adatoms on Pt(111) can be controlled through hydrogenation. This process is reversible as the H atoms can be desorbed one by one with the STM tip. Clean cobalt atoms on Pt(111) have $S \approx 1$, an out-of-plane easy magnetization axis, and a large magnetic anisotropy of 9.3 ± 1.6 meV [1]. After exposure to H_2, two complexes are formed and identified as CoH and CoH_2. Their differential conductance reveals inelastic features which strongly depend on their adsorption site. We identify the origin of these features using isotopic substitution of H with D and external magnetic fields up to 8 T. On the fcc site, the CoH complex displays spin excitations and the CoH_2 complex shows a Kondo signature. The magnetic field behavior of these features identifies the fcc-adsorbed CoH species as effective spin $S_{eff} = 2$, and the CoH_2 complex as $S_{eff} = 3/2$, with a Landé g factor very close to 2 in both cases. Surprisingly, the hydrogen-induced spin increase of the surface-adsorbed complex is opposite to the decrease in the free molecule. The control of the spin of an individual atom through H adsorption and desorption opens up new possibilities to tailor the magnetism of a system down to the atomic scale.

The Pt(111) was prepared with cycles of Ar^+ sputtering followed by flash annealing at 1400 K at a base pressure of 3×10^{-10} mbar. Co atoms were deposited on the surface in the scanning tunneling microscope at $T = 17$ K with a flux

of 4×10^{-4} ML/s using a commercial electron beam evaporator with a 99.995% purity Co rod. All measurements were performed with our home-built 0.4 K scanning tunneling microscope equipped with an 8.5 T out-of-plane superconducting magnet [2,21]. Images were obtained in constant current mode at the tunnel voltages (V) and currents (I_t) given in the figure captions. The dI/dV spectra were acquired with a lock-in amplifier using the given peak-to-peak bias modulation V_{mod}.

Figure 1(a) presents a STM image of the Pt(111) surface after deposition of a Co coverage $\Theta = 3.5 \times 10^{-3}$ monolayers (ML) with minute amounts of residual H in the cryostat. The most prominent features are the protrusions attributed to single Co atoms. As evidenced by the profile taken along the green line [Fig. 1(b)], the protrusions have three distinct apparent heights of 1.85 ± 0.06 Å, 1.52 ± 0.03 Å, and 1.44 ± 0.01 Å, given in decreasing order of abundance of the respective species. Although the apparent heights depend on the bias and the tip apex, they always exhibit significant differences and the same order as above by which the three species can unequivocally be distinguished. The highest protrusions are identified as clean Co from the agreement between their scanning tunneling spectroscopy (STS) features with the ones from literature

[22,23], which also allows us to discern hcp- and fcc-adsorbed atoms, see Fig. 1(c). As in previous studies [22,23], and in contrast to Ref. [24], no peculiar low-energy features could be evidenced in the STS spectra of Co/Pt(111) (note that we use much smaller tunnel currents than the authors of Ref. [24]).

Hydrogen exposure and tip-induced sequential H desorption [2] identify the second most abundant species as CoH and the most shallow and least abundant one as CoH_2. In particular, we note the following. (i) The characteristic features of CoH disappear after stabilizing the STM tip over them at $|V| = 174 \pm 8$ mV and $I_t = 100$ pA (see Supplemental Material [25]), turning them into clean Co adatoms. This dehydrogenation with the STM tip is independent of the voltage polarity and is irreversible. The CoH_2 complexes are dehydrogenated in the same conditions as CoH, and are usually switched into CoH at slightly lower voltages. (ii) After exposure to H_2 gas, the abundance of CoH and CoH_2 increases noticeably; thus, we conclude that they correspond to hydrogenated Co complexes. (iii) Those complexes identified as CoH_2 tend to become more abundant with increasing H_2 exposure than the complexes identified as CoH. Furthermore, triangle-shaped complexes are also observed at higher H_2 exposures. These complexes do not exhibit any noticeable feature in STS (see Supplemental Material [25]) and can be changed into CoH_2, CoH, or clean Co with increasing tip-sample voltage. We therefore identify this last type as CoH_3. This assignment, and the tip-induced H dissociation, are in agreement with recent results for CoH_n on Ag(111) [15]. Note that a similar procedure can also be used to reversibly adsorb and desorb H from Fe adatoms (see Supplemental Material [25]).

The differential conductance spectra of CoH and CoH_2 display prominent steps symmetric to zero bias and with conductance variations up to 20% caused by inelastic transitions of the adsorbate complexes, see Figs. 1(d) and 1(e). The threshold energies of these steps are given in Table I. These energies, as well as the shape of the spectra, strongly depend on the adsorption site. All four species present at least two distinct inelastic excitations each. In addition, the spectrum of fcc-adsorbed CoH reveals an extra pair of inelastic steps at 0.39 ± 0.05 meV, whereas the fcc-adsorbed CoH_2 complex displays a very large zero-bias peak.
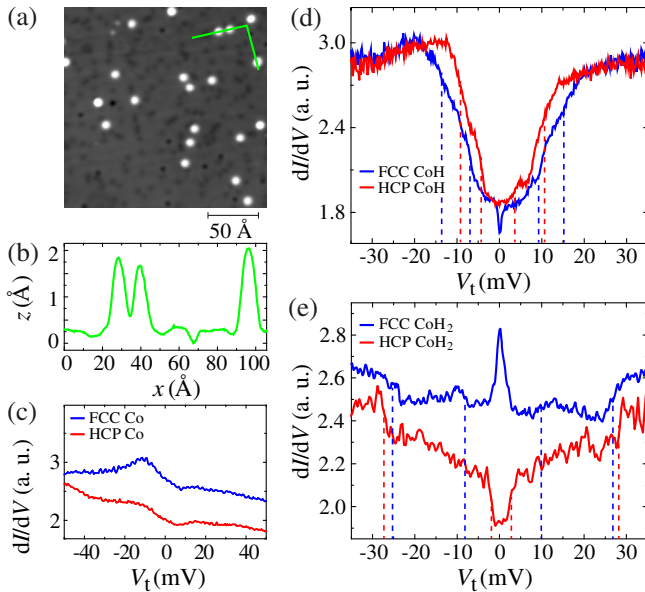

FIG. 1 (color online).   (a) STM image of Co adatoms on Pt(111) ($V_t = -50$ mV, $I_t = 100$ pA, $T = 4.4$ K, $\Theta = 3.5 \times 10^{-3}$ ML, shallow depressions are subsurface C atoms, $\Theta = 2.5 \times 10^{-2}$ ML, pronounced depressions are surface C atoms, $\Theta = 2.3 \times 10^{-3}$ ML). (b) Apparent height profile along the line marked in (a). (c) Differential conductance (dI/dV) spectra of fcc- and hcp-adsorbed Co adatoms ($V_t = -50$ mV, $I_t = 1$ nA, $V_{\mathrm{mod}} = 2.8$ mV, $T = 4.4$ K). (d) dI/dV spectra of CoH complexes on both adsorption sites ($V_t = -50$ mV, $I_t = 1$ nA, $V_{\mathrm{mod}} = 0.3$ mV, $T = 0.4$ K). (e) dI/dV spectra of CoH_2 complexes ($V_t = -45$ mV, $I_t = 0.75$ nA, $V_{\mathrm{mod}} = 1$ mV, $T = 0.4$ K). Dashed lines mark the inelastic conductance steps.

TABLE I.   Energies of inelastic conductance steps (meV) of CoH and CoH_2 complexes on both adsorption sites. ($T = 0.4$ K, $B = 0$ T).

CoH fcc	CoH hcp	CoH_2 fcc	CoH_2 hcp
$0.39 \pm 0.05^{\mathrm{a}}$	$\cdots$	0^{a} (peak)	$\cdots$
7 ± 1.5	4.5 ± 1	9.5 ± 1.5	2.4 ± 0.9
14 ± 1.5	8.5 ± 1.5	25.5 ± 0.7	26.5 ± 1.5

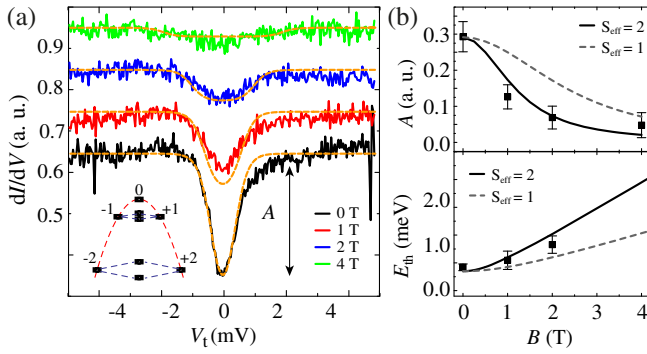[a]This energy shifts with an applied magnetic field.

FIG. 2 (color online). (a) Magnetic field dependence of dI/dV spectra of fcc-adsorbed CoH. A parabolic background was subtracted from each spectrum ($V_t = -5$ mV, $I_t = 0.25$ nA, $V_{\mathrm{mod}} = 500~\mu$V, $T = 0.4$ K). Dashed orange lines show simulated spin-excitation spectra. Inset: schematics of the corresponding quantum levels labeled by m. The effects of uniaxial and transverse anisotropies are represented by red and blue dashed lines, respectively. (b) Experimental (dots) and calculated (solid line) transition amplitudes A and threshold energies E_{th} between the lowest two states of a $S_{\mathrm{eff}} = 2$ multiplet. The best fit obtained with $S_{\mathrm{eff}} = 1$ is shown as dashed line for comparison ($g = 2.1$, $D = -9$ meV, $E = 0.175$ meV).

To determine the origin of these inelastic features, we employed isotopic substitution of H with D and magnetic fields up to 8 T along the surface normal. We first focus on the CoH case. The larger conductance steps displayed by this complex on both adsorption sites show no field dependence (see Supplemental Material [25]) identifying their vibrational origin. However, they show no isotope effect. Therefore, we attribute them to a frustrated translation of the metal atom [2,12,13].

The pair of conductance steps observed at ±0.39 meV for fcc-adsorbed CoH show a clear magnetic field dependence as evidenced in Fig. 2(a). Similar to Fe atoms on Cu$_2$N/Cu(100) [29], the energy of this excitation increases with field, see Fig. 2(b). At the same time, its amplitude decreases until it vanishes at about $B = 4$ T. In order to rationalize the magnetic behavior of this complex, we use the effective spin Hamiltonian [30]:

$$\hat{\mathcal{H}}_{\mathrm{spin}} = g\mu_B \hat{\vec{S}}_{\mathrm{eff}} \cdot \vec{B} + D\hat{S}_{\mathrm{eff}_z}^2 + E(\hat{S}_{\mathrm{eff}_x}^2 - \hat{S}_{\mathrm{eff}_y}^2), \quad (1)$$

where g is the electron Landé factor, $\vec{B}$ the magnetic field, D and E the uniaxial and transverse anisotropy parameters, and $\hat{\vec{S}}_{\mathrm{eff}}$, $\hat{S}_{\mathrm{eff}_x}$, $\hat{S}_{\mathrm{eff}_y}$, and $\hat{S}_{\mathrm{eff}_z}$ are the total effective spin operator and its projection along x, y, and z, whereby the axes are assigned such as to maximize $|D|$ and yield $E > 0$. The energies and eigenfunctions obtained from diagonalizing Eq. (1) are then used to simulate the spin-excitation spectra as described in Ref. [29]. The existence of a step at zero field and its disappearance with increasing field are indicative of a nondegenerate zero-field ground state doublet, which is only possible for an integer spin multiplet. Both, the transition energies and amplitudes are best

reproduced by $S_{\mathrm{eff}} = 2$, $g = 2.1 \pm 0.2$, $D = -3 \pm 1$ meV, and $E = 0.6 \pm 0.2$ meV with the z axis along the surface normal, see Fig. 2. The negative value of D indicates that the $m = \pm 2$ doublet is lowest in energy. This doublet is mixed by the E term and splits into two $m = 0$ singlets at $B = 0$, see inset of Fig. 2(a). Thus the ground state wave function contains $m = \pm 2$ and $m = 0$ components (see Supplemental Material [25]). In this scheme, spin excitations with $\Delta m = 0$ are allowed by the quantum overlap of these states [29]. An out-of-plane magnetic field lifts the mixing of the ground states; thus, the two $m = 0$ singlets gradually recover the $m = \pm 2$ behavior and further split under the Zeeman effect. Consequently, first order spin excitations between $m = \pm 2$ states which must satisfy the rule $\Delta m = 0, \pm 1$ [29] become forbidden and the inelastic transition is gradually quenched. Note that the observed behavior cannot be reproduced using threefold symmetric transverse terms, as they do not mix the states of the $m = \pm 2$ doublet [30]. Therefore, the presence of a twofold E term suggests an adsorption geometry of the CoH complex which breaks the C_{3v} symmetry of the surface.

A ground state with $S_{\mathrm{eff}} = 2$ is quite surprising for the CoH complex, with its S_{eff} being even higher than the spin of a free Co atom. Calculations for the free CoH molecules predict a $S = 1$ ground state multiplet, with the antiparallel coupling between the spins of the Co ($S = 3/2$) and the H atom ($S = 1/2$) [19]. These calculations further show that ferromagnetic alignment yielding the observed $S = 2$ becomes favored only upon an increase of the Co-H bond length by 10%. Our results suggest that the hybridization of the complex with the Pt(111) surface can favor a larger Co-H equilibrium distance and, consequently, a ferromagnetic coupling of Co and H spins. We finally note that only the transition between the lowest doublet is experimentally observed, whereas higher energy excitations are probably obscured by the intense vibrational features.

The exotic magnetic phase found for CoH is further modified upon the adsorption of an additional H atom. For the fcc-adsorbed species, we find a strong impact of isotopic substitution on the position of the conductance steps (this point was not investigated for hcp-adsorbed species). Upon D$_2$ exposure, two new complexes displaying inelastic steps at 18.0 ± 0.5 meV, respectively, 20.7 ± 0.4 meV are observed, see Fig. 3(a). These threshold energies are related to the CoH$_2$ mode at 25.5 ± 0.7 meV by ratios of $\sqrt{2}$ and $\sqrt{3/2}$, respectively. The lower conductance steps located at 10 ± 1.5 meV for CoH$_2$ shift to 8 ± 1 and 7 ± 1 meV, thus with comparable ratios [see also Fig. S5(b) in Supplemental Material [25], where these steps are seen more clearly). These numbers correspond to masses of 4, 3, and 2, consistent with the energies of bending vibrations of CoH$_2$, CoHD, and CoD$_2$, respectively. The presence of such modes further confirms the identification of this complex as CoH$_2$ and indicates a bent geometry rather than an axial alignment of the two H and the Co atoms. The bent geometry is expected for such a
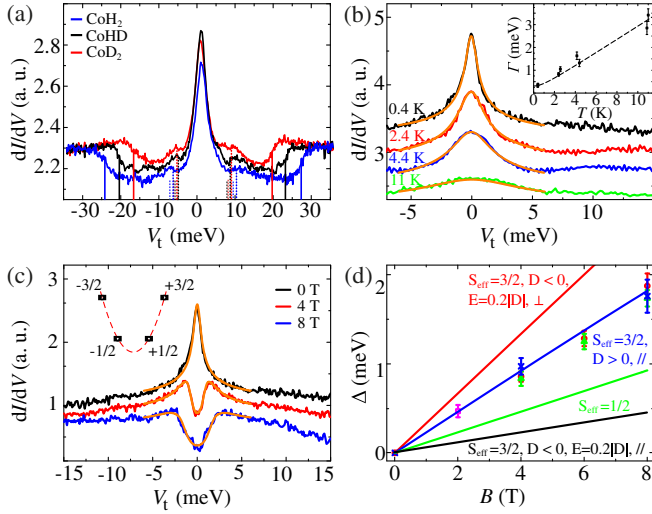
FIG. 3 (color online).   (a) Isotope shifts in conductance steps of fcc-adsorbed CoH_2, CoHD, and CoD_2. The energies at half the step height are marked with vertical lines. A parabolic background was subtracted from each spectrum ($V_t = -50$ mV, $I_t = 0.75$ nA, $V_{mod} = 1$ mV, $T = 4.4$ K). (b) Temperature dependence of the zero-bias peak and of its width (inset) of CoH_2. Orange lines: simulated dI/dV spectra, see text. (c) Field splitting of zero-bias peak of CoH_2 ($V_t = -15$ mV, $I_t = 0.1$ nA, $V_{mod} = 500$ μV, $T = 0.4$ K). Orange lines: simulated dI/dV spectra, see Supplemental Material [25]. Inset: quantum levels of an $S_{eff} = 3/2$ system with $D > 0$. (d) Field splitting of Kondo peak and spin-excitation step. Symbols are experiment and correspond to different CoH_2 complexes. Lines show the field splitting expected from Eq. (1) for the indicated spins and anisotropies, $g = 2$, $|D| = 3$ meV.

complex in a nonpurely uniaxial chemical environment [17]. None of the conductance steps found for fcc- and hcp-adsorbed CoH complexes show a variation with the magnetic field, confirming their vibrational nature (see Supplemental Material [25]).

The zero-bias peak of the fcc-adsorbed CoH_2 complexes splits in an external magnetic field and progressively broadens with temperature, see Figs. 3(b) and 3(c). These are the signatures of a Kondo system. The symmetric shape of the peak suggests that the quantum interference with the continuum of substrate electrons is negligible [31]. Therefore, we fit our spectra with the Frota-model [32] that gives best agreement with the experimental line shape among the approaches employed in the literature [31–35]. The many-body density of states reads

$$g_{Frota}(eV) = -\text{Re}\left(\sqrt{i\tilde{\Gamma}(T)/(i\tilde{\Gamma}(T) + eV)}\right), \quad (2)$$

where Re indicates the real part, and $\tilde{\Gamma}(T) = \sqrt{\Gamma(T)^2 + \Gamma_{tip}(T)^2}$ the peak width obtained from the quadratic sum of the intrinsic width and the tip temperature broadening. Simulated dI/dV spectra [orange lines in Fig. 3(b)] are then obtained by convoluting $g_{Frota}(eV)$ with

the lock-in modulation (see Supplemental Material [25]). As can be seen from inspection of the inset of Fig. 3(b), the intrinsic width is well fitted by $\Gamma(T) = (1.455/2)\sqrt{(2k_B T_K)^2 + (\alpha k_B T)^2}$ [36–38], where k_B is the Boltzmann constant. We obtain a Kondo temperature of $T_K = 2.7 \pm 0.5$ K and a slope of $\alpha = 4.6 \pm 0.6$. The small value of T_K indicates a relatively weak coupling with the Pt conduction electrons [35], possibly resulting from the H adsorption.

The Kondo peak splits and is progressively quenched in an out-of-plane magnetic field, see Fig. 3(c). In addition, two inelastic steps become evident and they also display a clear field-dependent energy threshold. In contrast to fcc-adsorbed CoH, these excitations are well visible even at $B = 8$ T, indicating that the transition takes places between states connected by a first-order spin-excitation. To extract the energy splitting Δ of the transition, we model the dI/dV spectra including the in-field behavior of both the Kondo peak and the spin excitation, as described in Supplemental Material [25] and Refs. [34,35]. The energy splitting clearly shows a linear dependence with B, see Fig. 3(d). A linear regression of the experimental values with $\Delta = g\mu_B B$ gives a surprisingly large g factor of 3.8 ± 0.2 thus excluding the simplest scenario of $S = 1/2$. A similar behavior is also observed at 4.4 K and for D-substituted complexes (see Supplemental Material [25]).

In order to further determine the spin state of the complex, we compare the observed splitting with the spin-excitation energies expected from Eq. (1) for a number of model effective spin systems, limiting our analysis to $S_{eff} \leq 2$ and assuming $g = 2$. The presence of a single zero-bias peak at zero field requires a degenerate ground state doublet connected by first-order spin excitations. These criteria allow excluding (i) any integer S_{eff} with finite magnetic anisotropy; (ii) purely uniaxial $S_{eff} = 3/2$ with $D < 0$. Moreover, any isotropic spin systems, as well as $S_{eff} = 3/2$ with $D > 0$ and out-of-plane z axis, give rise to the same behavior as $S = 1/2$ [20,39–41]. Among the remaining possibilities, only the case of $S_{eff} = 3/2$, $D > 0$ and the z axis parallel to the surface correctly reproduces the observed splitting. As also observed for Co atoms on $Cu_2N/Cu(100)$ [20], the fcc-adsorbed CoH_2 thus presents a $S_{eff} = 3/2$, an $m = \pm 1/2$ ground state [see inset of Fig. 3(c)], and an anomalous Zeeman splitting due to the specific spin and anisotropy energy landscape [42]. Unlike in Ref. [20], no higher energy spin-excitation between $m = 1/2 \rightarrow m = 3/2$ were observed; however, they might be obscured by the vibrational features. For a free CoH_2 in a bent geometry, two spin states $S = 1/2$ and $S = 3/2$ have been predicted, they exhibit H-Co-H bond angles of 90 and 65 degrees, respectively [17,18]. In the free molecule the first is the ground state. Similarly to CoH, we speculate that the high spin state results from an adsorption-induced geometrical distortion of the CoH_2 complex.

In conclusion, we show that CoH_n complexes adsorbed on Pt(111) fcc sites exhibit magnetic properties that are

unexpected from the respective gas phase molecules. No spin excitations were found for those complexes adsorbed on the hcp sites, confirming the large site-dependent interaction characteristic of the Pt(111) surface [43]. We find that the spin of a Co atom on Pt(111) can be modified in a controlled way through H adsorption. Since this is reversible, our results imply that one can reversibly manipulate the spin of a single adatom.

[1] P. Gambardella, S. Rusponi, M. Veronese, S. S. Dhesi, C. Grazioli, A. Dallmeyer, I. Cabria, R. Zeller, P. H. Dederichs, K. Kern, C. Carbone, and H. Brune, Science **300**, 1130 (2003).

[2] F. Donati, Q. Dubout, G. Autès, F. Patthey, F. Calleja, P. Gambardella, O. V. Yazyev, and H. Brune, Phys. Rev. Lett. **111**, 236801 (2013).

[3] I. G. Rau, S. Baumann, S. Rusponi, F. Donati, S. Stepanow, L. Gragnaniello, J. Dreiser, C. Piamonteze, F. Nolting, S. Gangopadhyay, O. R. Albertini, R. M. Macfarlane, C. P. Lutz, B. A. Jones, P. Gambardella, A. J. Heinrich, and H. Brune, Science **344**, 988 (2014).

[4] T. Eelbo, M. Waśniowska, M. Sikora, M. Dobrzański, A. Kozłowski, A. Pulkin, G. Autès, I. Miotkowski, O. V. Yazyev, and R. Wiesendanger, Phys. Rev. B **89**, 104424 (2014).

[5] F. Donati, L. Gragnaniello, A. Cavallin, F. D. Natterer, Q. Dubout, M. Pivetta, F. Patthey, J. Dreiser, C. Piamonteze, S. Rusponi, and H. Brune, Phys. Rev. Lett. **113**, 177201 (2014).

[6] J. Miguel, C. F. Hermanns, M. Bernien, A. Krüger, and W. Kuch, J. Phys. Chem. Lett. **2**, 1455 (2011).

[7] L. Liu, K. Yang, Y. Jiang, B. Song, W. Xiao, L. Li, H. Zhou, Y. Wang, S. Du, M. Ouyang, W. A. Hofer, A. H. Castro Neto, and H.-J. Gao, Sci. Rep. **3**, 1210 (2013).

[8] C. F. Hermanns, M. Bernien, A. Krüger, W. Walter, Y.-M. Chang, E. Weschke, and W. Kuch, Phys. Rev. B **88**, 104420 (2013).

[9] C. Wäckerlin, K. Tarafder, J. Girovsky, J. Nowakowski, T. Hählen, A. Shchyrba, D. Siewert, A. Kleibert, F. Nolting, P. M. Oppeneer, T. A. Jung, and N. Ballav, Angew. Chem., Int. Ed. **52**, 4568 (2013).

[10] N. Ballav, C. Wäckerlin, D. Siewert, P. M. Oppeneer, and T. A. Jung, J. Phys. Chem. Lett. **4**, 2303 (2013).

[11] P. Gambardella, S. Stepanow, A. Dmitriev, J. Honolka, F. M. F. de Groot, M. Lingenfelder, S. S. Gupta, D. D. Sarma, P. Bencok, S. Stanescu, S. Clair, S. Pons, N. Lin, A. P. Seitsonen, H. Brune, J. V. Barth, and K. Kern, Nat. Mater. **8**, 189 (2009).

[12] M. Pivetta, M. Ternes, F. Patthey, and W. D. Schneider, Phys. Rev. Lett. **99**, 126104 (2007).

[13] M. Ternes, A. J. Heinrich, and W.-D. Schneider, J. Phys. Condens. Matter **21**, 053001 (2009).

[14] F. D. Natterer, F. Patthey, and H. Brune, Surf. Sci. **615**, 80 (2013).

[15] D. Serrate, M. Moro-Lagares, M. Piantek, J. I. Pascual, and M. R. Ibarra, J. Phys. Chem. C **118**, 5827 (2014).

[16] S. J. Altenburg and R. Berndt, New J. Phys. **16**, 093047 (2014).

[17] P. E. M. Siegbahn, M. R. A. Blomberg, and C. W. Bauschlicher, Jr., J. Chem. Phys. **81**, 1373 (1984).

[18] N. O. Jones, M. R. Beltran, S. N. Khanna, T. Baruah, and M. R. Pederson, Phys. Rev. B **70**, 165406 (2004).

[19] C. N. Sakellaris and A. Mavridis, J. Chem. Phys. **137**, 034309 (2012).

[20] A. F. Otte, M. Ternes, K. v. Bergmann, S. Loth, H. Brune, C. P. Lutz, C. F. Hirjibehedin, and A. J. Heinrich, Nat. Phys. **4**, 847 (2008).

[21] L. Claude, Ph.D. thesis, Swiss Federal Institute of Technology Lausanne, 2005, http://infoscience.epfl.ch/record/49882.

[22] Y. Yayon, X. Lu, and M. F. Crommie, Phys. Rev. B **73**, 155401 (2006).

[23] F. Meier, L. Zhou, J. Wiebe, and R. Wiesendanger, Science **320**, 82 (2008).

[24] T. Balashov, T. Schuh, A. F. Takács, A. Ernst, S. Ostanin, J. Henk, I. Mertig, P. Bruno, T. Miyamachi, S. Suga, and W. Wulfhekel, Phys. Rev. Lett. **102**, 257203 (2009).

[25] See Supplemental Material at http://link.aps.org/supplemental/10.1103/PhysRevLett.114.106807, which also contains Refs. [26–28], for details about the reversible hydrogen adsorption process, the absence of field dependence for higher energy excitations, as well as the model of the Kondo line shape at zero and finite magnetic fields.

[26] J. Appelbaum, Phys. Rev. Lett. **17**, 91 (1966).

[27] P. Anderson, Phys. Rev. Lett. **17**, 95 (1966).

[28] J. Appelbaum, Phys. Rev. **154**, 633 (1967).

[29] C. F. Hirjibehedin, C.-Y. Lin, A. F. Otte, M. Ternes, C. P. Lutz, B. A. Jones, and A. J. Heinrich, Science **317**, 1199 (2007).

[30] A. Abragam and B. Bleaney, *Electron Paramagnetic Resonance of Transition Ions* (Clarendon Press, Oxford, 1970).

[31] U. Fano, Phys. Rev. **124**, 1866 (1961).

[32] H. O. Frota, Phys. Rev. B **45**, 1096 (1992).

[33] A. F. G. Wyatt and R. H. Wallis, J. Phys. C **7**, 1279 (1974).

[34] R. H. Wallis and A. F. G. Wyatt, J. Phys. C **7**, 1293 (1974).

[35] Y. Zhang, S. Kahle, T. Herden, C. Stroh, M. Mayor, U. Schlickum, M. Ternes, P. Wahl, and K. Kern, Nat. Commun. **4**, 2110 (2013).

[36] K. Nagaoka, T. Jamneala, M. Grobis, and M. F. Crommie, Phys. Rev. Lett. **88**, 077205 (2002).

[37] The numerical prefactor 1.455/2 is employed to obtain the correct zero-temperature limit for the Frota intrinsic width $\Gamma(0) = 1.455 T_K$.

[38] H. Prüser, M. Wenderoth, P. E. Dargel, A. Weismann, R. Peters, T. Pruschke, and R. G. Ulbrich, Nat. Phys. **7**, 203 (2011).

[39] C. Romeike, M. R. Wegewijs, W. Hofstetter, and H. Schoeller, Phys. Rev. Lett. **96**, 196601 (2006).

[40] R. Žitko, R. Peters, and T. Pruschke, Phys. Rev. B **78**, 224404 (2008).

[41] N. Roch, S. Florens, T. A. Costi, W. Wernsdorfer, and F. Balestro, Phys. Rev. Lett. **103**, 197202 (2009).

[42] R. Žitko, R. Peters, and T. Pruschke, New J. Phys. **11**, 053003 (2009).

[43] A. A. Khajetoorians, T. Schlenk, B. Schweflinghaus, M. dos Santos Dias, M. Steinbrecher, M. Bouhassoune, S. Lounis, J. Wiebe, and R. Wiesendanger, Phys. Rev. Lett. **111**, 157204 (2013).

Controlling the spin of Co atoms on Pt(111) by hydrogen adsorption

Q. Dubout,[1] F. Donati,[1] C. Wäckerlin,[1] F. Calleja,[1,2] M. Etzkorn,[1,3]
A. Lehnert,[1] L. Claude,[1] P. Gambardella,[1,4] and H. Brune[1]

[1] *Institute of Condensed Matter Physics (ICMP),*
École Polytechnique Fédérale de Lausanne (EPFL), Station 3, CH-1015, Switzerland
[2] *Madrid Institute for Advanced Studies, IMDEA Nanoscience,*
Calle Faraday 9, Campus Cantoblanco, E-28049 Madrid, Spain
[3] *Max Planck Institute for Solid State Research, Heisenbergstr. 1, 70569 Stuttgart, Germany*
[4] *Department of Materials, ETH Zürich, Hönggerbergring 64, CH-8093 Zürich, Switzerland*
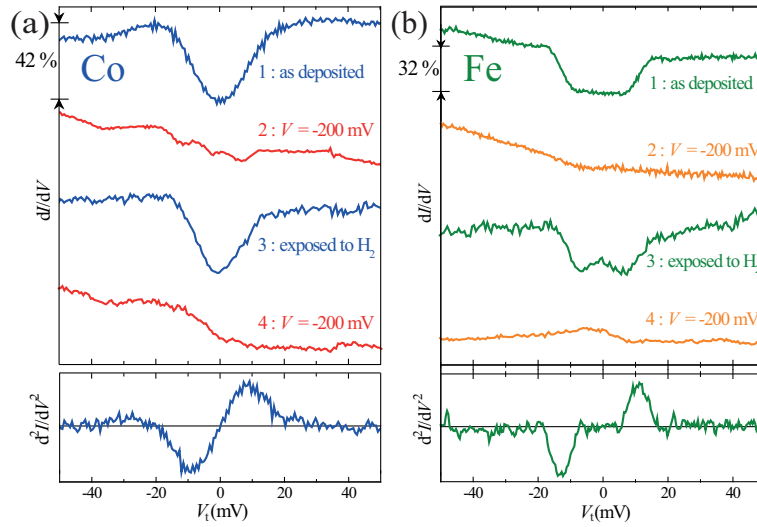
REVERSIBLE HYDROGEN ADSORPTION

FIG. S1. Sequence of dI/dV spectra acquired alternatingly on hydrogenated and clean Co (a), and Fe (b) adatom on Pt(111), as found directly after deposition (1), after a voltage pulse at -200 mV (2), after exposure to H_2 (3), and after a final -200 mV pulse (4) ($V_t = -50$ mV, $I_t = 1$ nA, $V_{mod} = 2.8$ mV, $T = 4.4$ K). Both Co and Fe hydrogenated adatoms display inelastic features, evidenced as peaks in d^2I/dV^2. The curve displayed is the numerical derivative of (1)). Note that these experimental conditions (temperature and lock-in modulation) do not allow to detect the low energy spin-excitation found for Fe atoms on Pt(111) in Ref. [43].

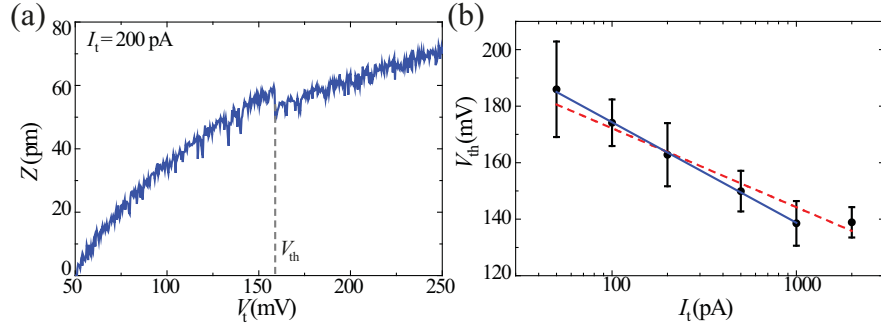## THRESHOLD VOLTAGE FOR HYDROGEN DESORPTION

FIG. S2. (a) Vertical displacement $z(V)$ curve acquired on top of a CoH complex. Hydrogen desorption is seen as a sharp downward step, as indicated by the grey dashed line ($I_t = 200$ pA, $T = 4.4$ K). (b) Hydrogen desorption voltage versus tunnel current. Each data point corresponds to the average V_{th} at which a jump in z was observed while ramping the voltage at constant current. Average over 10 CoH complexes. The solid blue line is a linear fit to the first five points and the dashed red line is a fit to the six points. The threshold V_{th} decreases exponentially with I_t, until it reaches a minimum value of about 140 mV.
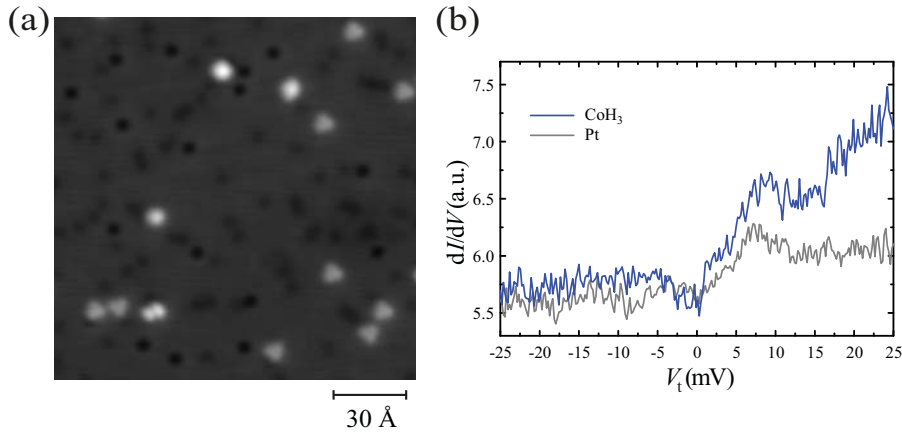
COBALT TRIHYDRIDE

FIG. S3. (a) STM image of a Co/Pt(111) sample that has been exposed to more H_2. Most of the CoH_n complexes appear as triangles with two possible orientations ($V_t = -50$ mV, $I_t = 83$ pA, $T = 4.4$ K). (b) dI/dV spectrum of a triangular CoH_3 complex. A spectrum acquired directly over the Pt(111) surface is also shown for comparison ($V_t = -25$ mV, $I_t = 0.5$ nA, $V_{mod} = 1$ mV, $T = 4.4$ K).
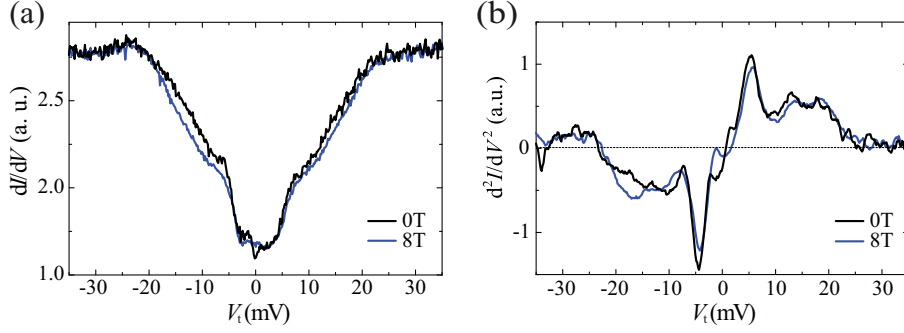
ABSENCE OF FIELD DEPENDENCE FOR HIGHER ENERGY EXCITATIONS

FIG. S4. (a) dI/dV spectra of two similar fcc-adsorbed CoH complexes at 0 and 8 T applied perpendicularly to the sample ($V_t = -45$ mV, $I_t = 0.75$ nA, $V_{mod} = 1$ mV, $T = 0.4$ K). (b) numerical derivative of (a).
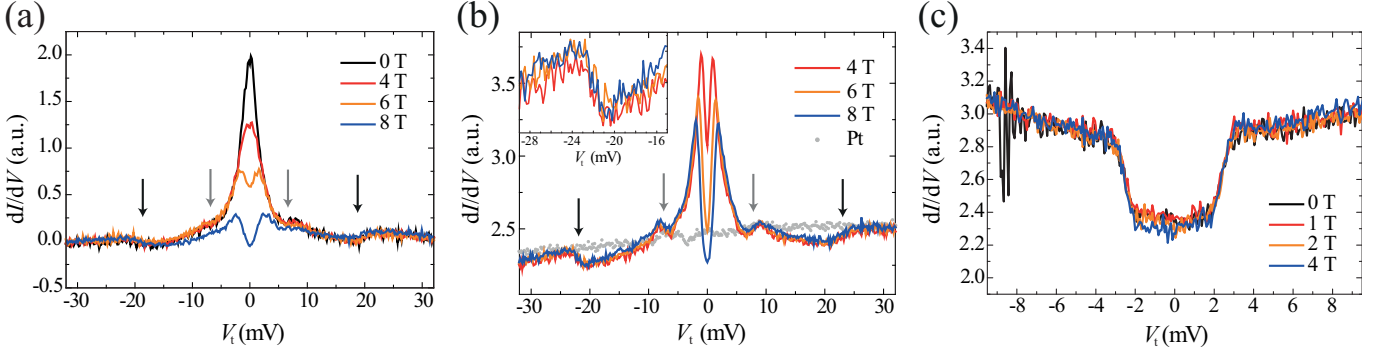

FIG. S5. (a) dI/dV spectra obtained over a fcc-adsorbed CoD$_2$ complex while applying an out-of-plane magnetic field ranging between 0 and 8 T. A parabolic background was subtracted from each spectrum ($V_t = -50$ mV, $I_t = 0.75$ nA, $V_{mod} = 1$ mV peak-to-peak, $T = 4.4$ K). (b) A similar series of spectra acquired on a CoHD complex at $T = 0.4$ K. A spectrum obtained on clean Pt(111) is shown for reference. Inset: magnification of an inelastic step emphasizing its insensitivity to external magnetic fields. In (a) and (b), the black and gray arrows mark the inelastic vibrational features whose energy thresholds allow distinguishing the CoHD and CoD$_2$ complexes from the CoH$_2$ one. None of these modes display field-dependence. (c) dI/dV spectra obtained over a hcp-adsorbed CoH$_2$ complex while applying an out-of-plane magnetic field ranging from 0 to 4 T ($V_t = -10$ mV, $I_t = 0.25$ nA, $V_{mod} = 500\,\mu$V, $T = 0.4$ K).

EIGENSTATES OF THE SPIN HAMILTONIAN FOR FCC-ADSORBED COH

TABLE I. Projection onto a m-states basis of the first two eigenstates of fcc-adsorbed CoH complexes obtained diagonalizing Eq. 1 of the main text with $S = 2$, $g = 2.1$, $D = -3$ meV, and $E = 0.6$ meV.

$B = 0$ T	$m = +2$	$m = +1$	$m = 0$	$m = -1$	$m = -2$
Ψ_0	0.697	0	-0.166	0	0.697
Ψ_1	0.707	0	0	0	-0.707
$B = 4$ T	$m = +2$	$m = +1$	$m = 0$	$m = -1$	$m = -2$
Ψ_0	0.083	0	-0.120	0	0.989
Ψ_1	0.988	0	-0.117	0	-0.097

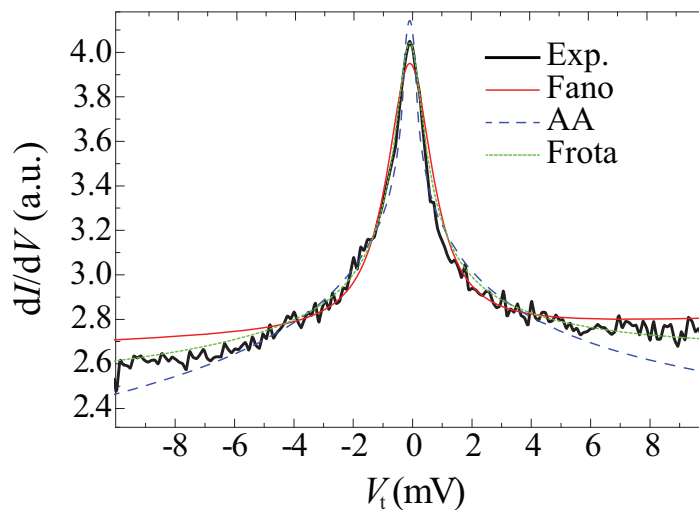## KONDO LINESHAPE IN ABSENCE OF A MAGNETIC FIELD

FIG. S6. dI/dV spectrum obtained over a fcc-adsorbed CoH$_2$ complex at 0 T and 0.4 K. $V = -15$ mV, $I_t = 0.1$ nA, $V_{mod} = 500\,\mu$V. Fits are based on the Frota, Fano and Anderson-Appelbaum models (Eqs. (S1), (S3), (S2)). A linear background is added to the fits.

In Fig. S6, least-square fits based on the Fano, Frota and Anderson-Appelbaum (AA) models [31–35] are compared. Equation (S1) gives the expression for the many-body density of states (DOS) of a Fano resonance [31]:

$$g_{Fano}(E) = \frac{(E/\Gamma_{Fano} + q)^2}{(E/\Gamma_{Fano})^2 + 1},\tag{S1}$$

with the linewidth Γ_{Fano}, and the Fano parameter q. In the Anderson-Appelbaum (AA) model [33–35], the many-body DOS is given by:

$$g_{AA}(E) = \left[\int_{-\omega_0}^{\omega_0} \frac{f(E')}{E - E'}\,dE' * \frac{df(E)}{dE}\right],\tag{S2}$$

with $f(E) = (1 + \exp[E/(k_B T)]))^{-1}$ being the Fermi-Dirac distribution, $[a(x) * b(x)]$ the convolution between $a(x)$ and $b(x)$, and ω_0 the cutoff energy for the integration. Using $\omega_0 = 100$ meV, we evaluated $g_{AA}(E)$ numerically for different temperatures T including a correction $-ln(1 + E/\omega_0)$ which compensates for ω_0 not being infinitely large [33] and stored the precomputed results for later use in the numerical fits.

The many-body DOS for the Frota model [32] is given in Eq. (S3)

$$g_{Frota}(E) = -Re(\sqrt{i\widetilde{\Gamma}/(i\widetilde{\Gamma} + E)}),\tag{S3}$$

with Re being the real part and $\widetilde{\Gamma}$ the peak linewidth. Simulated dI/dV spectra are then obtained convoluting the corresponding many-body DOS with the lock-in voltage modulation V_{mod}:

$$dI/dV(eV) \propto \left[g(E = eV) * e\sqrt{(V_{mod}^2 - V^2)}\right],\tag{S4}$$

where the function $g(E = eV)$ may be chosen to be $g_{AA}(E)$, $g_{Fano}(E)$ or $g_{Frota}(E)$. The Fano-lineshape fails to reproduce the tails of Kondo-resonance. The AA-model partially reproduces the tails of the Kondo resonance but yields a too narrow lineshape at the Kondo-peak. The Frota model best reproduces the Kondo lineshape, see Fig. S6.

In order to extract the Frota intrinsic linewidth Γ as a function of the temperature, we subtract the contribution of the tip thermal broadening in a quadratic approximation $\Gamma = \sqrt{\widetilde{\Gamma}^2 - \Gamma_{tip}^2}$. Here, we assume the tip thermal broadening Γ_{tip} to be proportional to the half-width-half-maximum of the derivative of Fermi-Dirac distribution $W_{FD} = \frac{1}{2}3.5k_BT$. More precisely, $\Gamma_{tip} = W_{FD}/2.54$, where the factor $1/2.54$ is due to the ratio between the Frota intrinsic width and the corresponding half-width-half-maximum [35, 38].

KONDO LINESHAPE IN APPLIED MAGNETIC FIELD

The expression for the conductance in applied magnetic field $\sigma(E)$ is [26–28, 33–35]:

$$\sigma(E) = \sigma_1(E) + \sigma_2(E),$$

$$\sigma_1(E) = c_1 \left[\frac{1}{3} + \frac{2}{3} \sum_{i,f;i \neq f} \rho_i(T) \left[\Theta(\frac{\Delta_{if} + E}{k_BT}) + \Theta(\frac{\Delta_{if} - E}{k_BT}) \right] \right],$$

$$\sigma_2(E) = c_2 \sum_{i,f;i \neq f} \rho_i(T) \left(\left[\Theta(\frac{\Delta_{if} + E}{k_BT}) + \Theta(\frac{\Delta_{if} - E}{k_BT}) \right] g(E) \right.$$

$$+ \left[\Theta(\frac{\Delta_{if} + E}{k_BT}) + \frac{1}{2} \right] g(E + \Delta_{if})$$

$$+ \left. \left[\Theta(\frac{\Delta_{if} - E}{k_BT}) + \frac{1}{2} \right] g(E - \Delta_{if}) \right).$$

(S5)

Here, $\rho_i(T) = (\exp[-E_i/(k_BT)])/(\sum_i \exp[-E_i/(k_BT)])$ is the thermal occupation of the spin in state i, $\Theta(x) = [1 + (x - 1)\exp(x)][1 - \exp(x)]^{-2}$ is the thermally broadened step-function, and Δ_{if} is the energy separation of the spin states i, f. The ratio of the prefactors c_1/c_2 sets the relative amplitudes of the spin excitation (σ_1) and the Kondo (σ_2) contributions to the conductance. Again, the function $g(E)$ may be chosen to be $g_{AA}(E)$, $g_{Fano}(E)$ or $g_{Frota}(E)$. Fits in Fig. 3(d) of the manuscript are obtained using $g(E) = g_{Frota}(E)$. Finally, simulated dI/dV spectra are then obtained convoluting the conductance σ with the lock-in voltage modulation:

$$dI/dV(eV) \propto \left[\sigma(E = eV) * e\sqrt{(V_{mod}^2 - V^2)} \right].$$

(S6)